15

Manufacturing of sapphire capillaries for fiber-optic instruments in laser medical applications

© I.A. Shikunova, D.O. Stryukov, Yu.N. Zubareva, I.N. Dolganova, S.L. Shikunov, V.N. Kurlov

Osipyan Institute of Solid State Physics RAS (ISSP RAS), Chernogolovka, Russia

e-mail: sh_irina@issp.ac.ru

Received December 11, 2024

Revised December 12, 2024

Accepted December 12, 2024

Sapphire needle capillary irradiators have been developed for interstitial laser therapy and surgery on a base of thin crystalline tubes with a monolithic needle at the working end. The sapphire capillary protects located inside quartz fiber which deliver laser radiation (including high-power) from chemical and/or mechanical damage, and also transforms the axial beam coming out of the fiber into a diffuse distribution for irradiating of tumors of varying sizes and locations. In addition to the geometry of the external surfaces of the irradiator, the shape of the transition from the tubular part of the capillary to the monolithic one (through which the radiation from the quartz fiber enters the monolithic needle end) has an influence on the angular distribution of radiation in the beam. This paper explores how different factors of growth process affect the ability to control the geometry of the transition area — the shape of the channel's bottom. The parameters of the radiation beam emitted from the needle-tipped irradiator were assessed based on the geometry of the transition region. The analysis demonstrates that with a conical monolithic tip, for typical sphericity values of the channel bottom, a partially collimated or focused beam is generated, spreading from the needle tip into the tissue volume. It has been demonstrated that to enhance the resolution of devices utilizing sapphire components with enclosed capillary channels, precise micro-scale control of the geometry and surface quality of the irradiator is essential.

Keywords: shaped sapphire, EFG /Stepanov technique, fiber-optic instruments, laser-induced thermo-therapy, photodynamic therapy, focusing.

DOI: 10.61011/EOS.2025.05.61641.18-25

Introduction

Sapphire is widely used as an optical material for manufacturing of products resistant to complex influences due to the unique combination of physical and chemical properties of sapphire [1–3]. Laser therapy and surgery using optical elements made of sapphire are accompanied by combined physical effects on tissues or continuous monitoring of their parameters using all available optical methods [4].

Quartz fiber light guides are usually used to transmit broadband or laser radiation in laser medicine and biophotonics [5]. Sapphire contact elements can be used in fiber light guides in the form of end attachments of various shapes that focus or scatter radiation, transform the beam into a lateral, annular, etc. [6,7]. elements can also have longitudinal channels closed on one side inside them, which are used to accommodate quartz optical fibers for various purposes [8]. The distal ends of the fibers, protected from contact with the tissue, can be brought directly to the object of exposure, while the sapphire element forms the required radiation distribution in malignant neoplasms of various nosologies and localization. Examples of such devices include sapphire interstitial irradiators with microfocus [9,10], a sapphire scalpel with tumor boundary detection [11,12], and a neuroprobe for aspiration of glial tumors with fluorescent diagnostics [13],

sapphire cryoapplicators with the ability to determine the depth of freezing of biological tissue by optical methods directly during cryodestruction [14–17], sapphire terahertz endoscope [18], a neuroport for phototeranostics [19].

The beams of diagnostic or affecting radiation delivered by a quartz fiber with a flat end primarily pass through the interface "air—sapphire" in the considered devices at the site of transition from the tubular part of the capillary to the monolithic part (hereinafter, for simplicity, we will call it the bottom of the channel). The high transparency, low number of defects, and smoothness of the crystal's growth surface allow radiation to pass through this surface with low losses. The formation of its curvature, which occurs in most cases, remains unexplored.

At the moment, there is a need to study the process of channel bottom formation. This is also relevant due to the tendency to reduce the size of the irradiators themselves and the objects exposed to radiation, when a small deviation in the shape of each surface can significantly affect the resulting radiation distribution. Solving this issue will make it possible to reasonably improve the characteristics of the developed irradiators, as well as develop tools for new areas of laser medicine and biophotonics. The purpose of this work was to study the process of growing sapphire capillaries with the ability to control the geometry of the channel bottom. Two types of needle capillaries were selected as objects of study: 2 mm in diameter with a

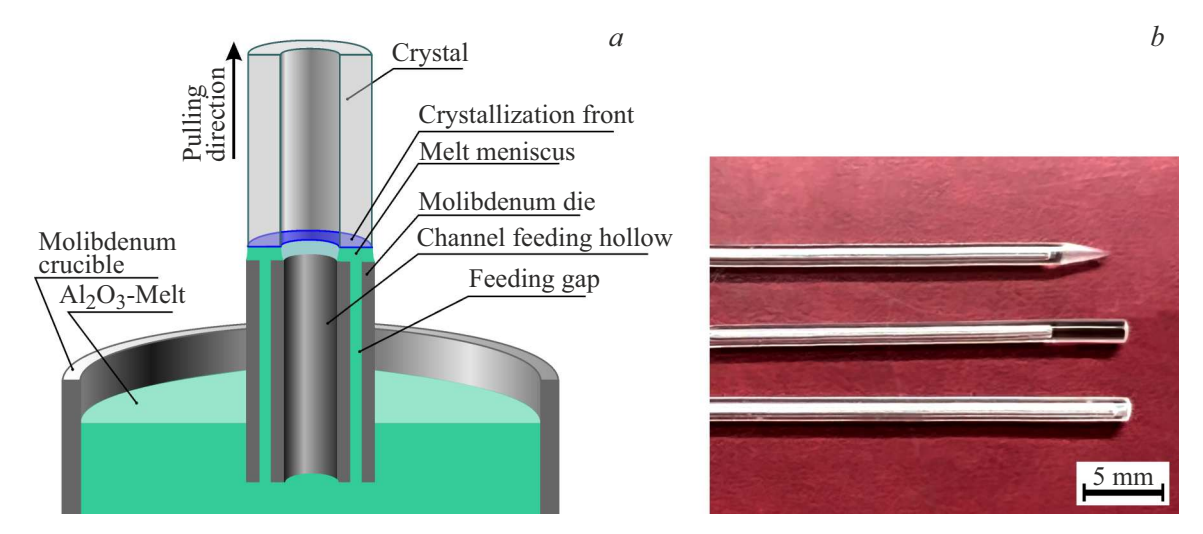


Figure 1. (a) The scheme of growing a sapphire capillary from a melt using the EFG/Stepanov's method, (b) a photograph of sapphire capillaries closed at one end.

channel diameter of 0.7 mm and 1.6 mm in diameter with a channel diameter of 1 mm. The dependence of the change in the beam parameters with an increase in the curvature of the channel bottom for the common conical shape of the monolithic part of the sapphire needle capillary is shown.

Growth of sapphire capillaries of variable cross-section from a melt

The shaped sapphire crystals with extended capillary channels were grown from a melt using the EFG (edge-defined, film-fed growth) [20–23] technique based on the concept of A.V. Stepanov [24]. The shape of the cross-section of the grown crystal is determined by the shape of a thin melt column (meniscus) enclosed between the upper end surface of the die and the crystallization front. The aluminum oxide melt rises from the crucible to the working edge of the wetted molybdenum mold through an annular channel located in it due to capillary forces, Fig. 1, a.

For the possibility of changing the crystal cross-sectional profile (closing or opening the channel), various designs of the molybdenum die have been developed to achieve optimal temperature distribution in the crystallization zone. Additional possibilities of changing the pressure above the channel-forming hole of the die were used to form and maintain the channel size, which made it possible to control not only the closing, but also the re-formation of the channel's in the crystal.

The sapphire capillaries were grown using an induction heating unit equipped with a highly sensitive crystal weight sensor. The cross-section of the sapphire capillary and the state of the crystallization front was controlled using an automatic control system with a weight sensor, the principles of which are described in Ref. [25].

Sapphire crystals grown by the Verneuil method were used as the initial charge. Sapphire capillaries (Fig. 1, b)

were grown in the crystallographic direction [0001] in a protective argon atmosphere under pressure 1.0-1.3 atm, the pulling rate varied in the range of 50-150 mm/h. The length of the sapphire capillaries was 150-200 mm. Crystals of shorter length (10-30 mm) with several cycles of transitions from the tubular part to the monolithic and back were grown in some cases.

To obtain a sapphire capillary with a low defect rate, it is necessary to maintain a relatively high height of the meniscus of the melt at its outer diameter, provided that the meniscus engages with the edges of the die. On the other hand, in order to form and maintain a given size of the channel cross-section, in the meniscus and at the crystallization front it is necessary to shift the thermal conditions at the crystallization front to the supercooling region, at which the height of the meniscus of the melt has a minimum value. This is necessary to prevent the collapse of the canal because of increasing Laplace pressure in a meniscus melt with decreasing of radius of average curvature of meniscus surface (reducing of diameter of the channel) and increasing in meniscus height.

Several approaches were used to move from the tubular part of the capillary to the monolithic one. In the case of growing capillaries with a small ($\leq 0.7\,\mathrm{mm}$) channel diameter, an increase in the pulling rate and/or temperature in the crystallization zone was used, which led to an increase in the height of the meniscus of the melt, followed by closing the channel in the capillary. The pulling velocity decreased after transition to a monolithic part for obtaining an optically transparent zone with a low defect content. The temperature was increased after the crystal movement stopped to change the cross-section in the case of growing of a thin-walled capillary or a capillary with a channel's diameter of $> 0.7\,\mathrm{mm}$, which led to an increase in the height and volume of the meniscus of the melt and, as a

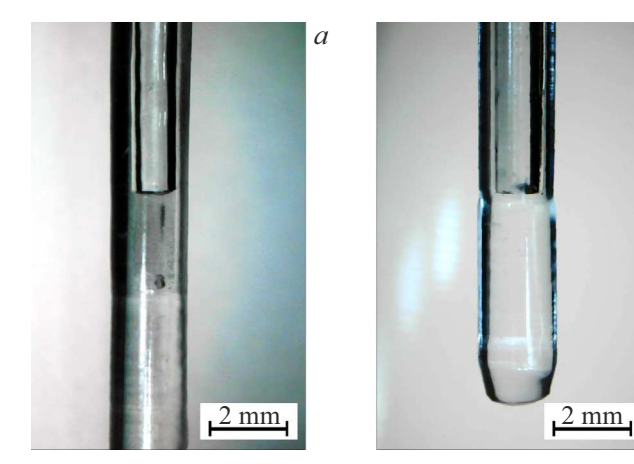


Figure 2. (a) Formation of bulk defects during channel closure by spontaneous crystallization of the melt, (b) the transition area after fusion of the defective fragment followed by rod growth.

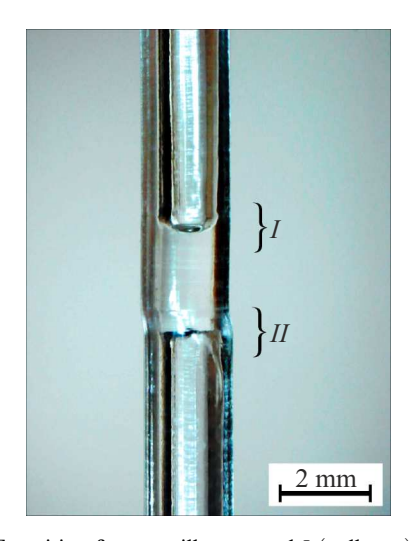


Figure 3. Transition from capillary to rod I (collapse) and channel formation II by temperature change in the crystallization zone.

result, the collapse of the channel. Further growth of the monolithic part was also carried out at a low pulling rate.

As another option for forming a transition from the tubular part of the capillary to the monolithic one, a rapid upward movement of the crucible with the melt was used. As the distance between the level of the working edges of the die and the surface of the melt in the crucible decreases, the modulus of the external static pressure in the meniscus changes, which leads to an increase in the height and volume of the meniscus of the melt, followed by the closure of the channel.

Also, a rapid separation of the capillary from the die was used as an alternative, as a result of which, part of the volume of the meniscus of the melt rose to a certain height into the crystal channel under the action of capillary forces and crystallized in it. The spontaneous crystallization of the melt in the channel of the sapphire capillary usually results

in the formation of pores and cavities, where the transverse size of the inclusions can reach the cross-sectional diameter of the channel itself, Fig. 2, a. A defect-free monolithic part of the crystal is obtained by the fusion of its defective fragment, followed by growing a rod of the required length at low rate, Fig. 2, b.

It is preferable to perform transitions of the "capillary-rod" shape for obtaining high-quality capillaries closed at one end. The most common procedure is to seed and expand the capillary, grow it in a stationary mode, collapse the channel in any convenient way and form a monolithic part of the required length. Fig. 3 shows a capillary with channel re-formation. The transition from the monolithic part of the capillary to the tubular one in the lower part of the photograph takes place due to a decrease in temperature in the crystallization zone.

Geometry of the bottom of closed channels in sapphire capillaries

In this paper, we examined two standard sizes of capillaries with an external diameter of $D=1.6\,\mathrm{mm}$ and a channel diameter of $d_\mathrm{c}=1.0\,\mathrm{mm}$ (the total number of shape transitions is 27, of which 14 — channel opening and 13 — collapse) and with an outer diameter of $D=2.0\,\mathrm{mm}$ and a channel diameter of $d_\mathrm{c}=0.7\,\mathrm{mm}$ (the total number of shape transitions is 119, of which 51 — channel formation and 68 — collapse). The first can be attributed to thinwalled capillaries $\frac{S}{D} < \left(\frac{1}{5} \ldots \frac{1}{4}\right)$, the second to thick-walled capillaries $\frac{S}{D} > \left(\frac{4}{10} \ldots \frac{3}{10}\right)$, where S is the wall thickness of the capillary. The samples of each size were divided into groups according to the method of shape transition. The shape of the bottom of the channels was evaluated separately for cases of opening and closing.

Both during the growing process, when observing the crystallization front through an optical system, and in annealed crystal blanks, shape transitions are clearly visible through the transparent crystal wall. At the same time, due to the high refractive index of sapphire, the apparent transverse size of the channel is 1.88 times its actual size. The longitudinal dimensions of the elements, including the deflection arrow of the bottom surface of the closed capillary channel a_{sph} , are not distorted. Various samples of longitudinal sections of small-section capillaries with shape transition were used to determine that the bottom of the channel in all cases has the correct shape of the body of rotation, while it can be described as spherical with a radius of curvature r. For a known channel diameter, the radius of curvature of the channel bottom is determined by the measured size a_{sph} , Fig. 4.

No noticeable difference of magnitude was observed in samples obtained by different transition methods, in the case of channel bottom formation with sphericity, so the average values were estimated for the entire group of capillaries divided into transitions "rod—capillary" and "capillary—rod" (opening and collapsing of the channel, respectively). The

№	D, mm	d _c , mm	Degree of curvature of the bottom of channel in case of opening	Degree of curvature of the bottom of channel in case of collapsing
1	1.6	1.0	0.86 ± 0.16	0.88 ± 0.23
2	2.0	0.7	0.75 ± 0.02	0.77 ± 0.05

The average value of the degree of curvature of the channel bottom $\rho = d_c/2r$ for two types of capillaries

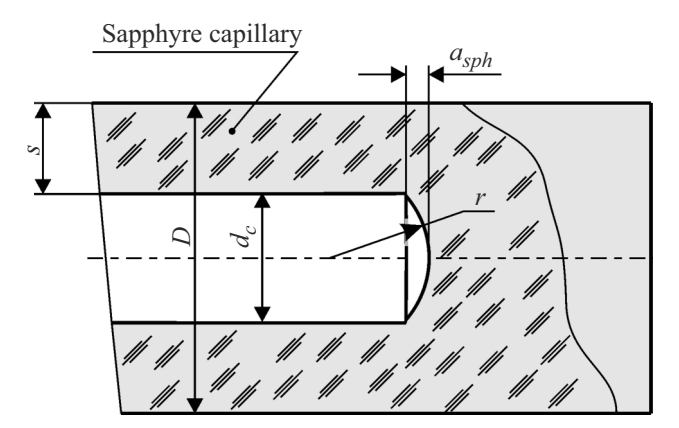


Figure 4. Diagram of a closed capillary.

cases when flat ends are formed (the curvature has large values and, accordingly, can be estimated with a significant error) were considered separately, while the frequency of their occurrence for a particular shaping method is different.

According to measurements of capillary samples of two standard sizes, the average degree of curvature of the bottom (the ratio of the channel radius to the radius of curvature of the bottom) is 0.75–0.88 (Table). The curvature of the bottoms is close to unity, i.e., on average, the shape of the surface is close to a hemisphere. When the channel collapses, it is slightly more curved than when it is opened. For a thin-walled capillary, the average degree of curvature of the bottom is less than in the case of a capillary with a thick wall.

The average curvature of the bottom of the channel with a diameter of $700\,\mu m$ was $480\,\mu m$. Thus, this surface is mostly significantly concave. This must be taken into account when using the bottom of the "as-grown" channel as the optical interface between air—sapphire in the path of propagating radiation both in the forward direction and in the opposite direction.

Conversion of optical beams by sapphire capillary needles with different channel bottom geometries

The revealed curved shape of the channel's bottom is a hemisphere or a rather convex end of the channel. Obviously, with a high refractive index of sapphire, the radiation beam coming out of the quartz fiber and passing through the interface with such a curvature will continue to follow with increased divergence. Numerical modeling for individual values of the curvature of the channel bottom shows a nonlinear decrease in the maximum energy of the laser beam (Fig. 5, a) and blurring of its spot (Fig. 5, b) as the shape of the channel bottom it changes from a flat (r infinitely large) to a hemispherical shape ($\rho=1$). At the same time, for the most frequently formed shapes of the channel bottom, small deviations in the degree of curvature of the shape significantly affect the beam parameters. Despite the fact that flat-ended irradiators are rarely in demand, nevertheless, this effect should be taken into account in devices, especially when using them for diagnostics with spatial resolution.

The most common geometry of the end of the irradiator is a cone, which allows obtaining a high concentration of light energy in a small area of the needle end. The radiation direction in this case is annular: the beam consists of groups of rays following at different angles to the axis of the irradiator, for which the condition of total internal reflection is consistently violated. Fig. 6, a shows the redistribution of radiation by a characteristic shaped sapphire needle with a tip angle of $2y = 50^{\circ}$ and a flat channel bottom working in combination with a quartz fiber dimeter $200 \,\mu\mathrm{m}$ with an aperture of $2\omega = 40^{\circ}$ placed in an aqueous medium. It is the high refractive index of the needle material $(n_s = 1.76)$ that makes it possible to preserve the beam transformation described above in an optically dense medium. The appearance and further increase of the bulge of the channel bottom in the direction of the cone leads to the fact that for the extreme rays in the laser beam, the condition of complete internal reflection ceases to be fulfilled, and part of the radiation forms a collimated or focused beam propagating from the tip of the needle deep into the medium. The transverse dimensions of such a light needle are tenths of a millimeter, Fig. 6, b. Fig. 6, c shows the distribution of laser radiation at the outlet of a similar needle in an aqueous medium. The size of the coagulated tissue zone obtained under the saline solution layer may not exceed 0.5 mm when the needle tip is removed from the tissue surface by 0.8-1.0 mm, Fig. 6, d (turkey liver ex vivo, irradiation continuous laser radiation with wavelength of $1.06 \mu m$, power 5 W for 30 s).

Discussion

Sapphire capillary irradiators are unique tools for surface and interstitial laser therapy and surgery. They can be combined with a wide range of radiation sources and fiber

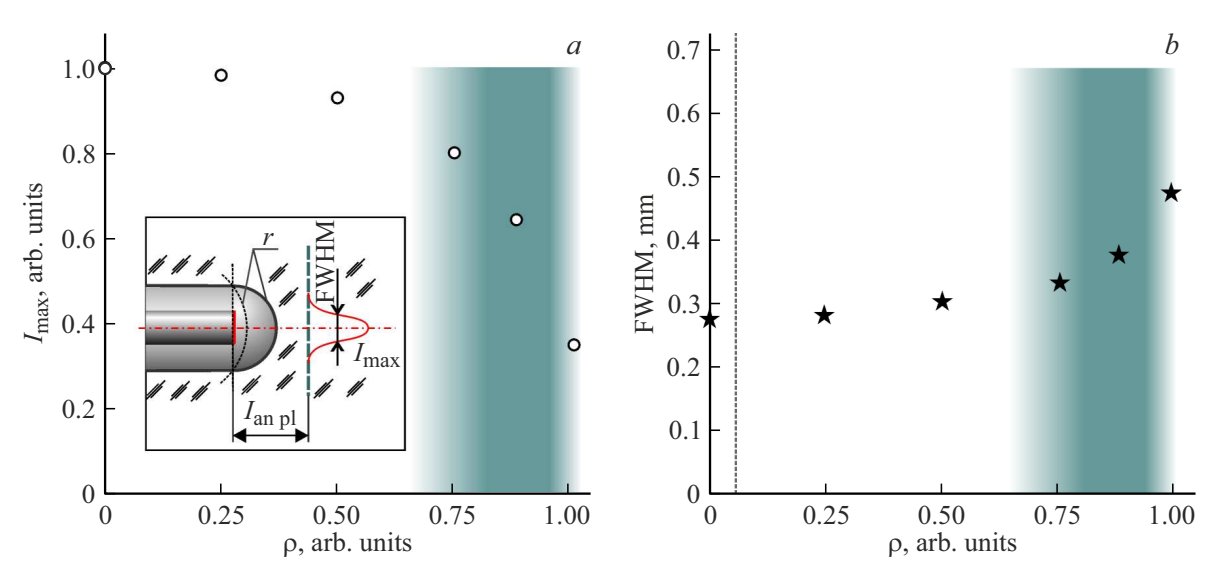


Figure 5. Dependence of the laser beam parameters on the degree of curvature of the channel bottom ρ for a capillary with a channel diameter of $d_c = 0.7$ mm when using quartz fiber with a diameter of $200 \,\mu\text{m}$ with an angular aperture of $2\omega = 40^\circ$: (a) energy maximum change along the I_{max} axis (circles), (b) change in spot size along the half-height of the Gaussian beam FWHM (star); distance from the radiating end of the fiber to the analysis plane $L_{\text{an pl}} = 2$ mm, the area of characteristic values is highlighted by dimming ρ .

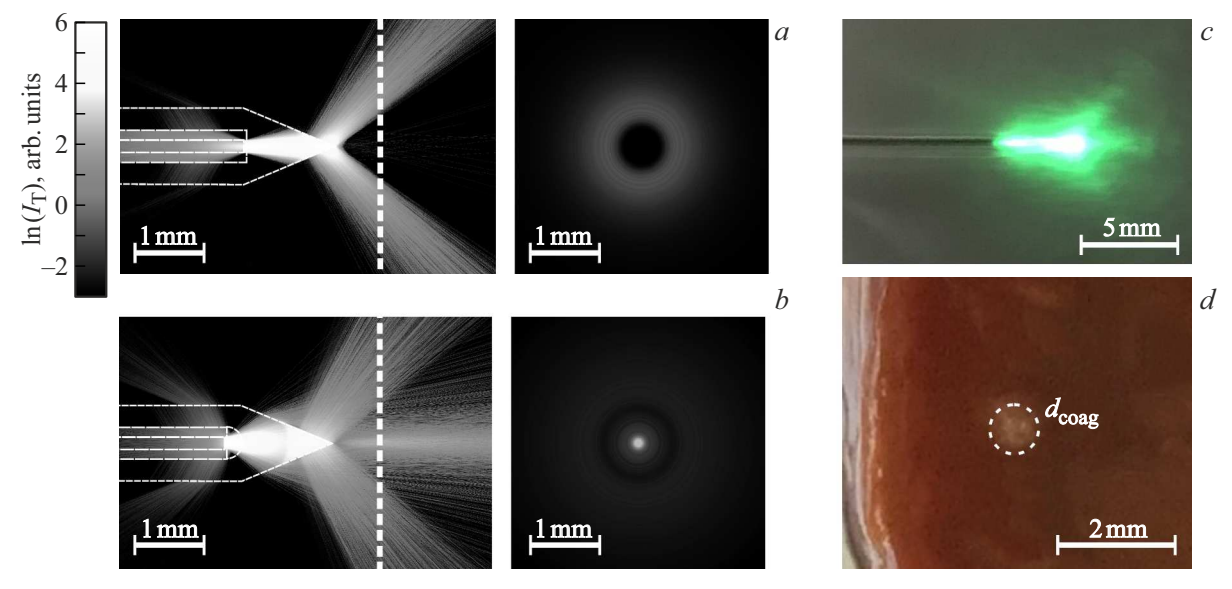


Figure 6. (a) Numerical Monte Carlo simulation (TracePro program) of the transformation of a Gaussian beam emerging from a fiber with a diameter of $200 \,\mu\text{m}$ with a numerical aperture of $800 \,\mu\text{m}$ must be an emerging from a fiber passing through the tip of the needle with a cone angle of $800 \,\mu\text{m}$ must be an adversary medium ($800 \,\mu\text{m}$) without scattering, (b) similar modeling for the bottom of a hemispherical channel, (with) photograph of a laser beam in an aqueous medium at the output of an irradiator with partially collimated radiation, (d) a region of coagulated tissue measuring $800 \,\mu\text{m}$, obtained on a liver sample immersed in saline solution.

light guides. With small transverse dimensions (the outer diameter of the capillary is not more than 2 mm), such irradiators can be manufactured with different shapes of their working ends to control the radiation pattern. In addition, the closed channel inside the needle, which is formed during crystal growth, may have a different bottom curvature. Since sapphire has a high refractive index, even small changes in the shape of the bottom of the channel

inside the needle noticeably change the distribution in the resulting beam, when a violation of the total internal reflection for a significant number of extreme rays in the volume of the monolithic conical tip leads to the appearance of axial beams. This is especially noticeable when working with an irradiator immersed in an optically dense medium, which is all biological media. The results of this study show that when obtaining closed capillaries using the EFG/Stepanov's method in the case of the formation of a convex in the direction of the needle end of the channel bottom, its shape is close to hemispherical. For this reason, when using sapphire needle irradiators, in addition to ringshaped diffusion beams, partially collimated and focused beams can also be formed in angular distributions.

The radiation direction from a small radiating area has a diffuse character in microfocusing irradiators using end cone nozzles or narrowing on quartz fiber. In our case, the needle-tipped irradiator forms a distribution in which part of the radiation propagates in the axial direction while maintaining a small spot size at a distance of several millimeters along the axis, which is of undoubted interest. This will allow using these needles for more effective local effects, for example, for coagulation of small metastases and cysts [26,27]. The point concentration of directed radiation near the tip of the needle in aqueous solutions can be used for photostimulation [28–30]. The use of various gels, including cooling ones, can further limit the area of laserinduced damage in the tissue in cases where it is important to ensure the preservation of the surrounding intact tissues. The same effect of local exposure can be achieved in lowscattering tissues or hollow organs.

The formation and maintenance of thin channels, as well as the control of the geometry of the channel bottom in sapphire closed capillaries, is reduced not only to optimizing the growth rates and temperature conditions in the crystallization zone, but also to using new approaches to the design of the forming device and the system for monitoring the state of the crystallization front. The shape of the bottom of a closed channel, close to a hemisphere, is the most common for capillaries with a medium to thick wall relative to the outer diameter. Small deviations in curvature can be predicted when choosing the technological parameters of cultivation, including the direction of transition, the method of channel collapse while maintaining high-quality monolithic and adjacent capillary parts.

Conclusion

The features of the technique of growing sapphire capillaries from a melt for surface and interstitial laser therapy and coagulation are analyzed. The process of forming the geometry of the channel bottom in sapphire capillary irradiators has been investigated and the shape of the radiation beam has been evaluated for different channel bottom geometries from flat to hemispherical. ways of implementing shape transitions in the growing of closed capillaries by the EFG/Stepanov's method are considered, the degree of curvature of the channel bottom is estimated for two typical sizes of sapphire capillaries used in irradiators. It has been found that even a slight change in the degree of curvature of the channel bottom significantly changes the divergence of the output beam and the nature of the radiation: the radiation patterns can vary significantly with different combinations of the channel bulge and the

angle of sharpening of the conical end. A special case of the geometry of a needle with a hemispherical end of the channel is given, where the beam has a narrow collimated part and a diffuse annular distribution of the rest of the radiation. This irradiator can be used for local tissue coagulation with a laser-induced coagulation zone size of no more than 1 mm without the risk of carbonization.

The results of this study have revealed the need to take into account the geometry of the channel bottom inside sapphire capillary irradiators. Search for technological ways to control the resulting shape of the bottom of a closed channel in the process of growing thin capillaries using the EFG/Stepanov's method is an urgent topic for future studies.

Funding

This study was supported by the Russian Science Foundation (RSF), project No. 24-29-00424.

Conflict of interest

The authors declare that they have no conflict of interest.

References

- V.N. Kurlov. Encyclopedia of Materials: Science and Technology, ed. by K.H.J. Buschow, R.W. Cahn, M.C. Flemings (Elsevier, 2001), p. 8259–8264.
 DOI: 10.1016/B0-08-043152-6/01478-9
- [2] E.R. Dobrovinskaya, L.A. Lytvynov, V. Pishchik. Sapphire: Material, Manufacturing, Applications (Springer-Verlag, N.Y., 2009). DOI: 10.1007/978-0-387-85695-7
- [3] V.A. Tatartchenko. Bulk Crystal Growth of Electronic, Optical & Optoelectronic Materials, ed. by P. Copper, S. Kasap, A. Willoughby (Wiley, 2005), p. 299–238. DOI: 10.1002/9780470012086.ch10
- [4] G. Katyba, K. Zaytsev, I. Dolganova, I. Shikunova, N. Chernomyrdin, S. Yurchenko, G. Komandin, I. Reshetov, V. Nesvizhevsky, V. Kurlov. Prog. Cryst. Growth Charact. Mater., 64 (4), 133–151 (2018).
 DOI: 10.1016/j.pcrysgrow.2018.10.002
- [5] M.R. Hamblin, Y. Huang. Handbook of Photomedicine (CRC Press, Boca Raton, FL, 2013). DOI: 10.1201/b15582
- [6] P. Greve. Applied laser medicine, ed. by H.P. Berlien,
 G.J. Müller (Springer, Berlin, 2003), p. 129–184.
 DOI: 10.1007/978-3-642-18979-1_4
- V. Knappe, A. Roggan, M. Glotz, M. Müller, J-P. Ritz, C-T. Germer, G. Mueller. Med. Laser Appl., 16 (2), 73–80 (2001). DOI: 10.1078/1615-1615-00013
- [8] G.M. Katyba, K.I. Zaytsev, I.N. Dolganova, I.A. Shikunova, N.V. Chernomyrdin, S.O. Yurchenko, G.A. Komandin, I. V. Reshetov, V. V. Nesvizhevsky, V. N. Kurlov. Prog. Cryst. Growth Charact. Mater., 64 (4), 133–151 (2018). DOI: 10.1016/j.pcrysgrow.2018.10.002
- [9] I.N. Dolganova, I.A. Shikunova, A.K. Zotov, M.A. Shchedrina, I.V. Reshetov, K.I. Zaytsev, V.V. Tuchin, V.N. Kurlov. J. Biophotonics, 13 (10), e202000164 (2020). DOI: 10.1002/jbio.202000164

- [10] I.N. Dolganova, I.A. Shikunova, G.M. Katyba, A.K. Zotov, E.E. Mukhina, M.A. Shchedrina, V.V. Tuchin, K.I. Zaytsev, V.N. Kurlov. J. Biomed. Opt., 24 (12), 128001 (2019). DOI: 10.1117/1.JBO.24.12.128001
- [11] I.N. Dolganova, D.A. Varvina, I.A. Shikunova, A.I. Alekseeva, P.A. Karalkin, M.R. Kuznetsov, P.V. Nikitin, A. K. Zotov, E.E. Mukhina, G.M. Katyba, K.I. Zaytsev, V.V. Tuchin, V.N. Kurlov. Laser. Surg. Med., 54 (4), 611–622 (2021). DOI: 10.1002/lsm.23509
- [12] V.N. Kurlov, I.A. Shikunova, A.V. Ryabova, V.B. Loschenov. Bulletin of the Russian Academy of Sciences: Physics, 73 (10), 1341–1344 (2009). DOI: 10.3103/S1062873809100086
- [13] I.A. Shikunova, D.O. Stryukov, S.N. Rossolenko, A.M. Kiselev, V.N. Kurlov. J. Cryst. Growth, 457, 265–269 (2017). DOI: 10.1016/j.jcrysgro.2016.08.062
- [14] I.N. Dolganova, A.K. Zotov, S.N. Rossolenko, I.A. Shikunova, S.L. Shikunov, K.B. Dolganov, K.I. Zaytsev, V.N. Kurlov. Crystals, 14 (4), 346 (2024). DOI: 10.3390/cryst14040346
- [15] I.A. Shikunova, I.N. Dolganova, A.A. Kuznetsov, E.E. Mu-khina, L.P. Safonova, K.I. Zaytsev, V.N. Kurlov. Cryobiology, 92, 278–279 (2020). DOI: 10.1016/j.cryobiol.2019.11.032
- [16] A.K. Zotov, A.V. Pushkarev, A.I. Alekseeva, K.I. Zaytsev, S.S. Ryabikin, D.I. Tsiganov, D.A. Zhidkov, I.A. Burkov, V.N. Kurlov, I.N. Dolganova. Sensors, 24 (11), 3655 (2024). DOI: 10.3390/s24113655
- [17] I.N. Dolganova, A.K. Zotov, L.P. Safonova, I.V. Reshetov, K.I. Zaytsev, V.N. Kurlov. J. Biophotonics, 16 (3), e202200288 (2023). DOI: 10.1002/jbio.202200288
- [18] G.M. Katyba, S.P. Lebedev, A.S. Kucheryavenko, I.N. Dol-ganova, N.V. Chernomyrdin, M.B. Burdanova, I.E. Spektor, M. Skorobogatiy, V.N. Kurlov, K.I. Zaytsev. Appl. Phys. Lett., 124, 243703 (2024). DOI: 10.1063/5.0207898
- [19] A.S. Sharova, Yu.S. Maklygina, G.M. Yusubalieva, I.A. Shikunova, V.N. Kurlov, V.B. Loschenov. J. Physics: Conference Series, 945, 12009 (2018). DOI: 10.1088/1742-6596/945/1/012009
- [20] H.E. LaBelle, A.I. Mlavsky. Mater. Res. Bull., 6 (7), 571–579 (1971). DOI: 10.1016/0025-5408(71)90006-7
- [21] H.E. LaBelle. Mater. Res. Bull., 6 (7), 581-589 (1971).DOI: 10.1016/0025-5408(71)90007-9
- [22] H.E. LaBelle. J. Cryst. Growth, **50** (1), 8-17 (1980). DOI: 10.1016/0022-0248(80)90226-2
- [23] P.I. Antonov, V.N. Kurlov. Crystallography Reports, 47 (1), S43-S52 (2002). DOI: 10.1134/1.1529958
- [24] A.V. Stepanov. Budushchee metalloobrabotki (Lenizdat, L., 1963), p. 130 (in Russian).
- [25] V.N. Kurlov, S.N. Rossolenko. J. Cryst. Growth, 173, 417–426 (1997). DOI: 10.1016/S0022-0248(96)00836-6
- [26] A. Shalabi, A. Ehab, S. F. Shalabi, G. Kugler, H.-J. Schäfers,
 T. Graeter. Nat. Sci. Rep., 14, 5988 (2024).
 DOI: 10.1038/s41598-024-56566-5
- [27] H. Fu, F. Luo, H. Zhao. J. Cosmet. Dermatol., **20** (9), 2805–2809 (2021). DOI: 10.1111/jocd.13994
- [28] B. Spagnolo, A. Balena, R. T. Peixoto. Nat. Mater., 21, 826-835 (2022). DOI: 10.1038/s41563-022-01272-8
- [29] V. Emiliani, E. Entcheva, R. Hedrich. Nat. Rev. Methods Primers, 2, 55 (2022). DOI: 10.1038/s43586-022-00136-4
- [30] A. Tsakas, C. Tselios, D. Ampeliotis, C. Politi, D. Alexandropoulos. Results in Optics, 5, 100168 (2021). DOI: 10.1016/j.rio.2021.100168

Translated by A.Akhtyamov